Electronic Supplementary Information

Quantitative multiplexing of uric acid and creatinine using polydisperse plasmonic nanoparticles enabled by electrochemical-SERS and machine learning

Tabitha Jones[a,b], Deyue Zhou[a,b], Jia Liu[a,b], Ivan P. Parkin[a], Tung-Chun Lee[a,b]

[a] Department of Chemistry, University College London, London, WC1H 0AJ
[b] Institute of Materials Discovery, University College London, London, WC1H 0AJ

Table of Contents

S1. Methodology

S1.1. Synthesis and fabrication

S1.1.1. Materials

Silver nitrate ($AgNO_3$), sodium citrate ($Na_3C_6H_5O_7$), uric acid ($C_5H_4N_4O_3$), creatinine ($C_4H_7N_3O$), (3-aminopropyl)triethoxysilane (APTES) ($C_9H_{23}NO_3Si$), acetic acid (CH_3COOH), urea (CH_4N_2O), potassium chloride (KCl), citric acid ($HOC(COOH)(CH_2COOH)_2$), albumin from human serum, ethanol (C_2H_6O), and acetone (C_3H_6O) were all purchased from Sigma-Aldrich/Merck. Sodium fluoride (NaF), sodium phosphate dibasic (NaH_2PO_4), and rhodamine 6G ($C_{28}H_{31}N_2O_3Cl$) were purchased from ARCOS Organics. Sodium chloride (NaCl) was purchased from VWR Chemical. All chemicals were used as received, and Milli-Q water was used in all experiments. The fluorine doped tin oxide (FTO) coated glass slides were purchased from Sigma-Aldrich.

S1.1.2. Synthesis of Ag NPs

To synthesise the silver nanoparticles, a standard citrate reduction was used following the Lee and Meisel method.[1] 36 mg of silver nitrate ($AgNO_3$) was dissolved in 200 ml H_2O and brought to the boil in a round-bottomed flask whilst stirring. Once boiling, 4 ml of a 1% sodium citrate ($Na_3C_6H_5O_7$) solution was added to the silver nitrate solution dropwise. Heating and stirring were maintained for an hour. A colour change from colourless to milky green/grey was observed which indicted successful nanoparticle formation. Once cool, the flask was wrapped in foil to prevent light degradation of the colloid solution.

S1.1.3. Preparation of APTES-coated FTO-coated glass

To improve the adhesion of the Ag NP film, a (3-Aminopropyl)triethoxysilane (APTES) coating was applied to FTO-coated glass electrodes. The FTO-coated glass electrodes were washed with soapy water and then ultrasonically cleaned for 20 minutes using ethanol, acetone, and Milli-Q water consecutively. The electrodes were then dried using a gentle stream of nitrogen gas. A 95% ethanol-5% water solution was prepared, and the pH was adjusted to 4.5 – 5.5 with approximately 10 µL 1 M acetic acid. APTES was added whilst stirring to give a 2% final concentration. The solution was then left for at least 5 minutes. The FTO-coated glass electrodes were dipped into the solution for 2 minutes and agitated gently. The electrodes were then dipped briefly in ethanol to remove excess APTES and left at room temperature overnight to cure the APTES layer.

S1.1.4. Preparation of synthetic urine

Synthetic urine (SU) which did not contain uric acid or creatinine was prepared according to the literature with modifications.[2,3] For 200 ml of SU, 2 g of urea, 1.04 g of NaCl, 0.9 g of KCl, 0.96 g of NaH_2PO_4, 0.08 g of citric acid, and 10 mg of albumin were dissolved in 200 ml of deionized water.

S1.2. Instrumentation

S1.2.1. UV-visible (UV-Vis) spectroscopy

UV-vis spectra of the colloidal Ag NP solution were acquired using a DH-mini Ocean Optics light source and a Flame S UV-vis ES Ocean Optics spectrometer. Milli-Q water was used to store the reference and background spectra. The colloidal Ag NP solutions were transferred into a 1 cm optical path length cuvette and placed in the spectrometer for measurement. A 10 ms integration time was used, with 300 scans to average, and a boxcar width of 3. The absorbance spectra were collected in a wavelength range of 180 - 880 nm.

S1.2.2. Transmission Electron Microscopy (TEM)

Images of the Ag NPs were obtained using a JEOL JEM-2100 transmission electron microscope with an Orius SC200 1 camera at an accelerating voltage of 200 kV. A 5 μL droplet of the sample NP solution was drop-cast onto a C-coated 300-mesh Cu grid, air-dried and then imaged. Particle sizing was performed using ImageJ software.

S1.2.3. Scanning Electron Microscopy (SEM)

Images of the Ag NP films were obtained using a JEOL JSM 6701 FEG-SEM at an accelerating voltage of 10 kV. The samples were coated with gold for 10 seconds using an Agar sputter coater.

S1.3. Machine Learning

S1.3.1. Dataset and pre-processing

The data analysis was performed using Python and the Scikit-learn library was used for all machine learning.[4] To pre-process the spectra for machine learning, they were first truncated to eliminate regions without significant Raman signals, removing measurements 500 cm^{-1} and above 1800 cm^{-1}. After trimming the spectra, asymmetric least squares (ALS) baseline correction was applied.[5] Then, standard normal variate normalisation was performed to give each spectrum a mean intensity of 0 and a standard deviation of 1.[6] For the multilayer perceptron models, the analyte concentrations were also scaled via min-max normalization so that all of the values were transformed into the range [0,1].

The dataset was randomly split into training (80%) and test (20%) datasets. Hyperparameter optimisation was performed on 5 K-fold splits of the training dataset. The performance of the model was assessed using the test dataset and the coefficient of determination, R^2, was calculated to evaluate the accuracy of the predictions.[7]

S1.3.2. Bayesian optimisation with Gaussian processes

Bayesian optimisation is a strategy that can be used to efficiently determine the optimal parameters for a machine learning algorithm.[8,9] In this work, Bayesian optimisation with Gaussian processes was used to find the optimal number of latent variables in the PLSR and

hidden layer architecture for the MLP. The PLSR could have between 5 and 65 latent variables and the MLP could have between 1 and 3 layers. Each layer could have 4, 8, 16, 32, 64 or 128 nodes. This results in 28,080 possible options. During the optimisation, a possible PLSR-MLP architecture was selected from these options. The performance of this PLSR-MLP model was then quantified by calculating the R^2 from 5 K-fold splits of the training dataset.[10] As the optimisation progressed, the selection started to converge. After 150 selections, the architecture that resulted in the highest R^2 was returned and this was used to build the final PLSR-MLP model.

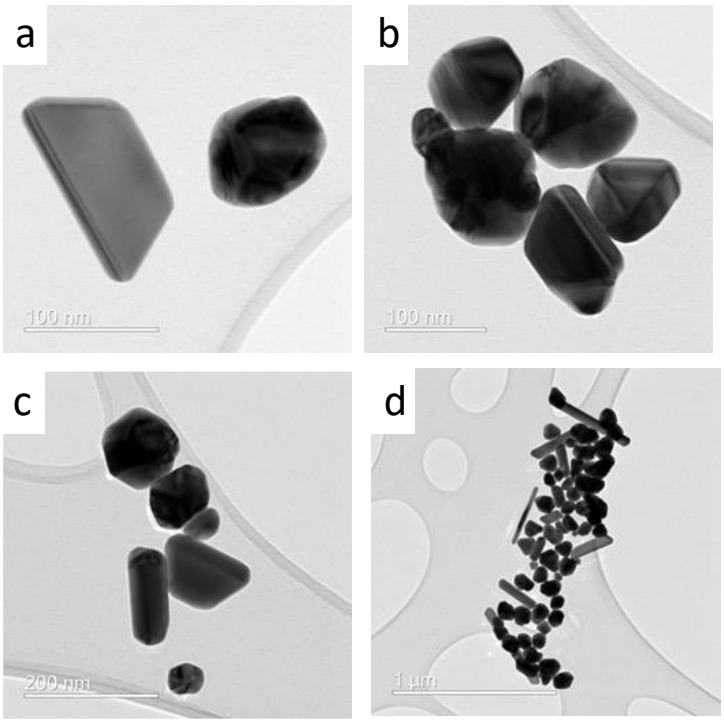

Fig. S1: TEM images of silver nanoparticles.

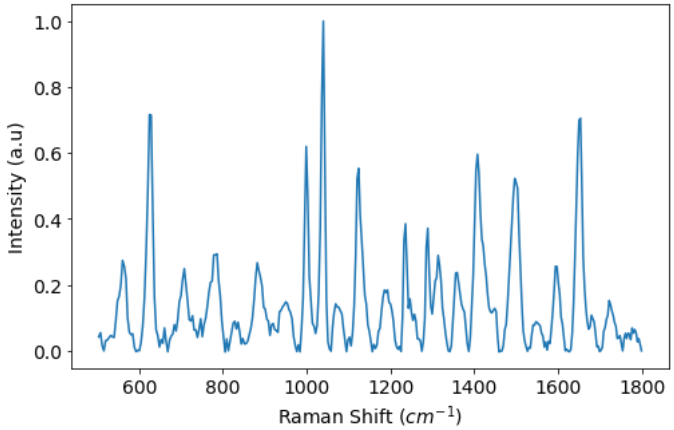

Fig. S2: Raman spectrum of uric acid powder.

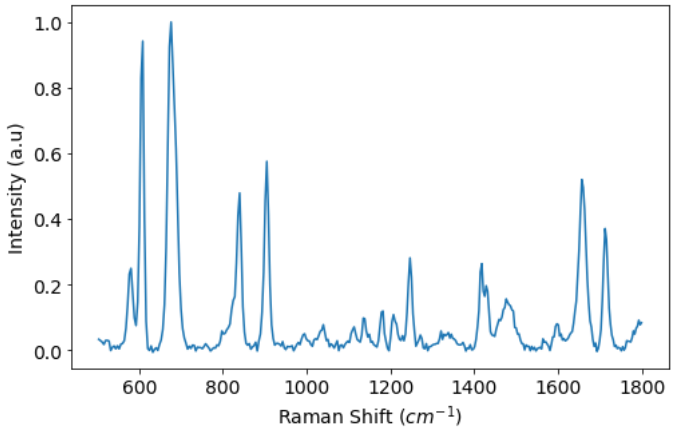

Fig. S3: Raman spectrum of creatinine powder.

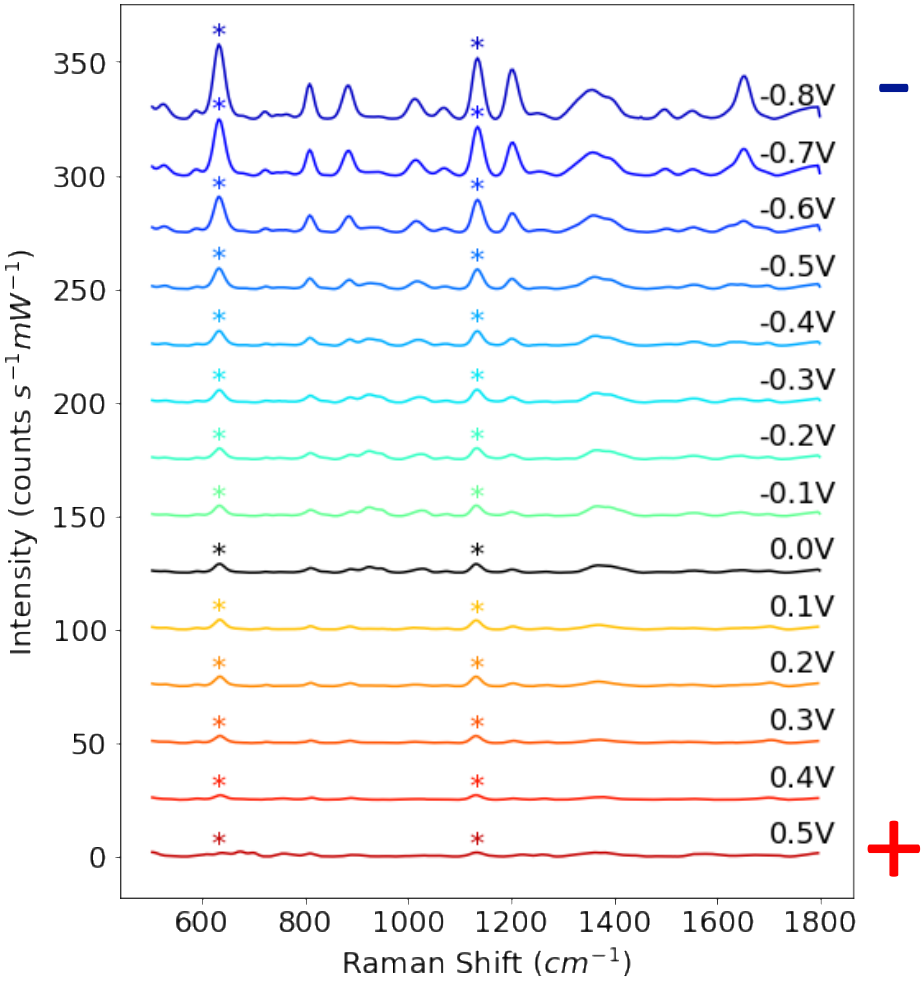

*Fig. S4: E-SERS spectra of 0.5 mM UA with 0.1 M NaF as the supporting electrolyte. The applied potential was stepped from 0 to 0.5 V and from 0 to -0.8 V in 100 mV increments. The characteristic UA peaks are indicated with a *. The spectra plotted are an average of 3 spectra recorded over 5 minutes (with spectra in the first 75 seconds removed to allow for equilibration). (RE: Ag/AgCl; WE: Ag NPs on FTO; CE: platinum plate).*

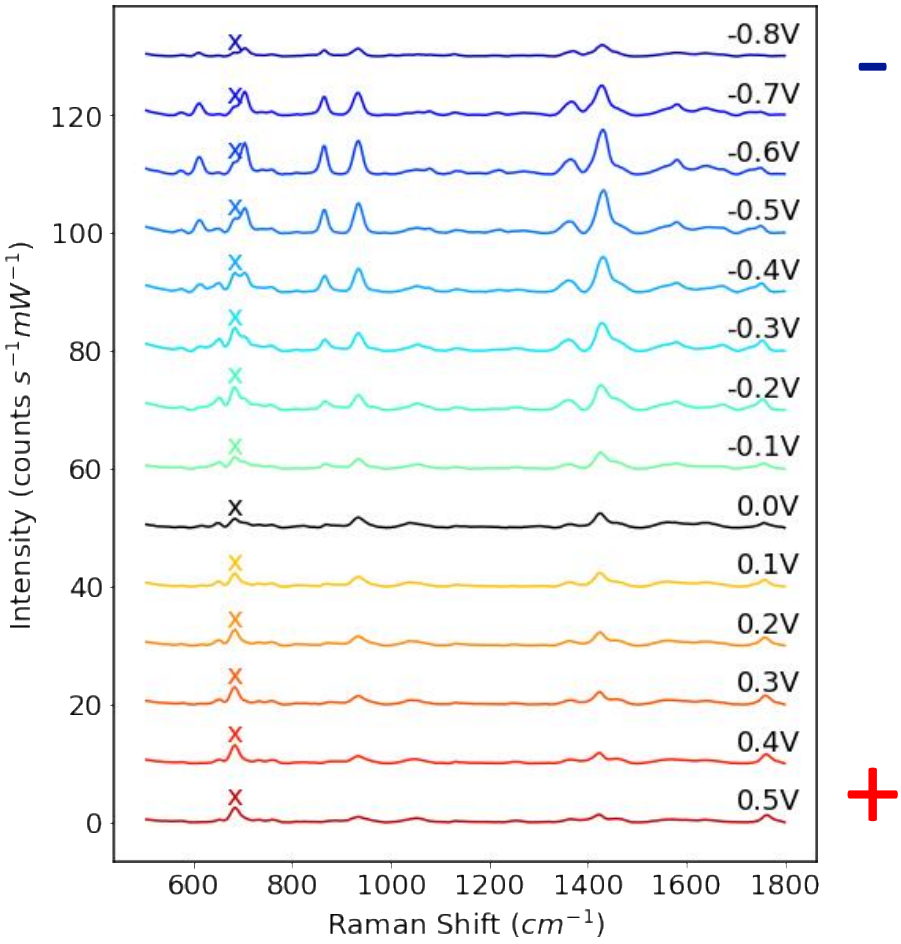

Fig. S5: E-SERS spectra of 0.5 mM $CRN_{(aq)}$. The applied potential was stepped from 0 to 0.5 V and from 0 to -0.8 V in 100 mV increments. The characteristic CRN peak is indicated with an x. The spectra plotted are an average of 3 spectra recorded over 5 minutes (with spectra in the first 75 seconds removed to allow for equilibration). (RE: Ag/AgCl; WE: Ag NPs on FTO; CE: platinum plate; supporting electrolyte: 0.1 M NaF).

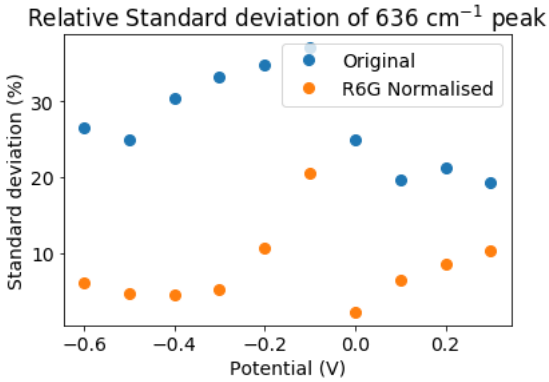

Fig. S6: The standard deviation of the characteristic uric acid peak at 636 cm^{-1} as a percentage of the mean peak height for the original and R6G normalised spectra. The standard deviation is calculated for 3 Ag NP/FTO electrodes which were submerged in a 0.1 mM UA + 0.01 mM R6G + 0.1 M NaF (aq) solution. (RE: Ag/AgCl; WE: Ag NPs on FTO; CE: Platinum plate).

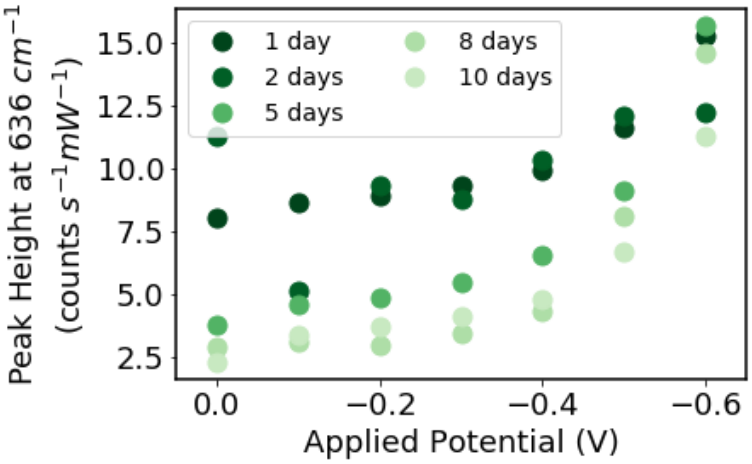

Fig. S7: The height of the characteristic uric acid peak at 636 cm^{-1} is plotted against the applied potential for multiple E-SERS scans of an aqueous solution containing 0.5 mM UA and 0.1 M NaF. The colour of the marker indicates the number of days since the Ag NP/FTO substrate was fabricated. A different substrate was used for each scan, and this was the first scan for each substrate. In each scan, the applied potential was stepped in the cathodic direction from 0 V to -0.6 V in 100 mV increments The reduction in the peak height with ageing is attributed to oxidation of the silver. (RE: Ag/AgCl; WE: Ag NPs on FTO; CE: platinum plate).

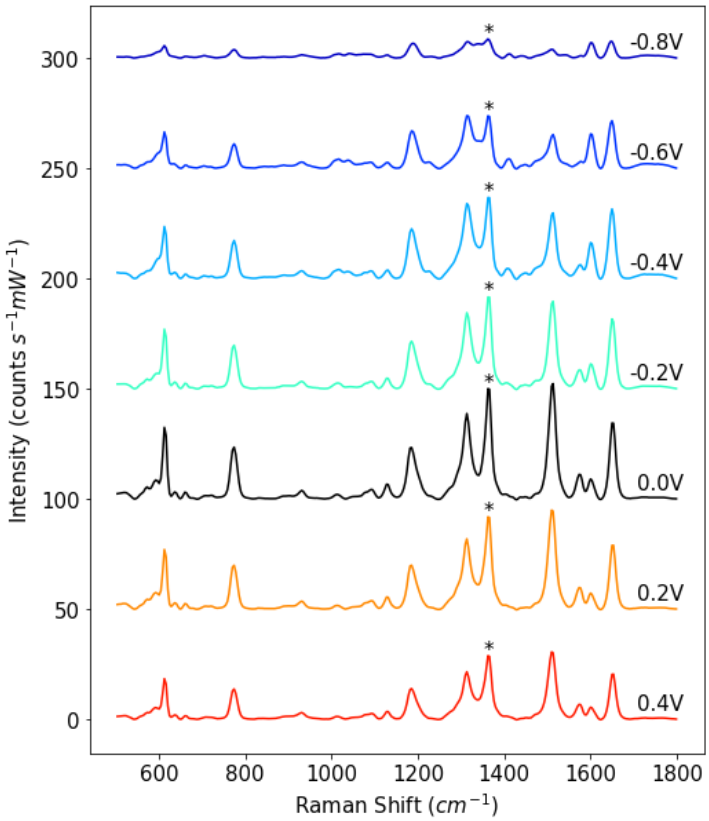

*Fig. S8: E-SERS spectra of a solution containing 10 μM R6G and 0.1 M NaF. The characteristic peak at 1362 cm^{-1} used for normalisation is indicated by a *. The applied potential was stepped in the anodic direction from 0 V to 0.4 V and then in the cathodic direction from -0.2 V to -0.8 V in 0.2 V increments. (RE: Ag/AgCl; WE: Ag NPs on FTO; CE: Platinum plate).*

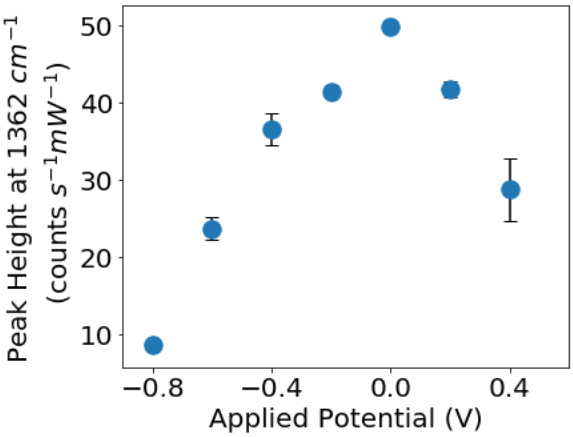

Fig. S9: The height of the characteristic R6G peak at 1362 cm^{-1} plotted against applied potential for a solution containing 10 µM R6G and 0.1 M NaF. (RE: Ag/AgCl; WE: Ag NPs on FTO; CE: Platinum plate).

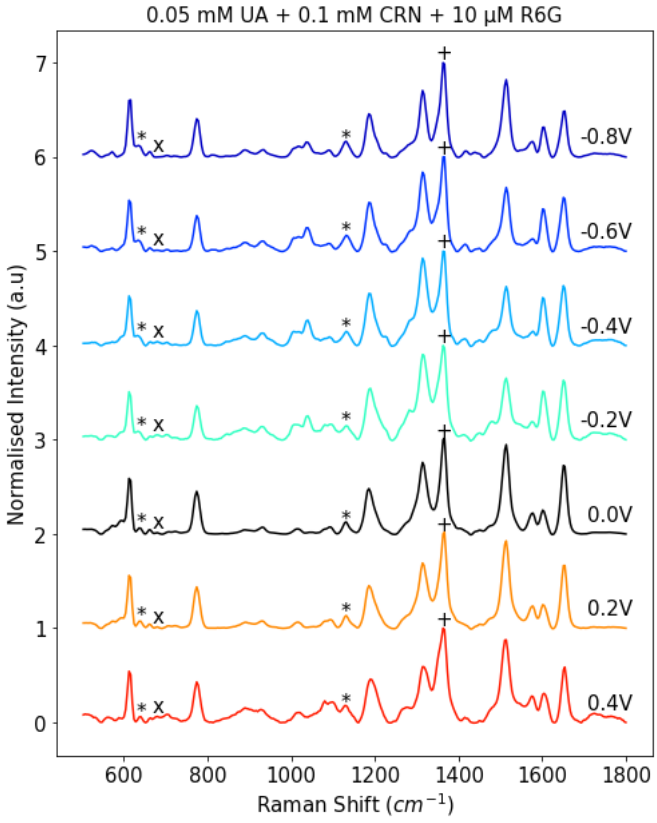

*Fig. S10: E-SERS spectra of a solution containing 0.05 mM UA, 0.1 mM CRN, 10 µM R6G and 0.1 M NaF. The characteristic R6G, uric acid, and creatinine peaks are indicated by a +, a *, and a x respectively. The applied potential was stepped in the anodic direction from 0 V to 0.4 V and then in the cathodic direction from -0.1 V to -0.8 V in 0.1 V increments. (RE: Ag/AgCl; WE: Ag NPs on FTO; CE: Platinum plate).*

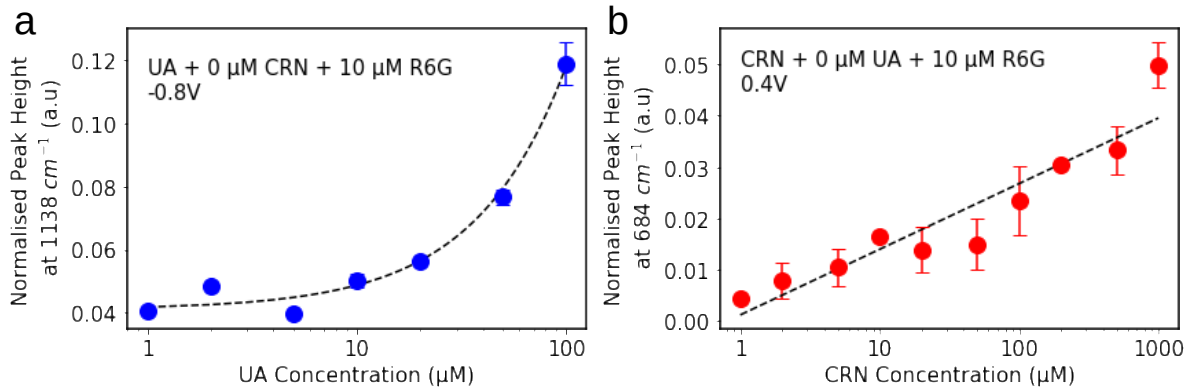

Fig. S11: (a) The R6G normalised peak height at 1138 cm^{-1} plotted against UA concentration for the spectra recorded at -0.8V. A linear relationship is fitted between UA concentration and the peak height for concentrations from 1 µM to 100 µM (R^2 = 0.988) and plotted on a log x-axis. (b) The R6G normalised peak height at 684 cm^{-1} plotted against CRN concentration for the spectra recorded at 0.4V. A linear relationship is fitted between log(CRN concentration) and the peak height for concentrations from 1 µM to 1000 µM (R^2 = 0.902) and plotted on a log x-axis. (RE: Ag/AgCl; WE: Ag NPs on FTO; CE: platinum plate; supporting electrolyte: 0.1 M NaF).

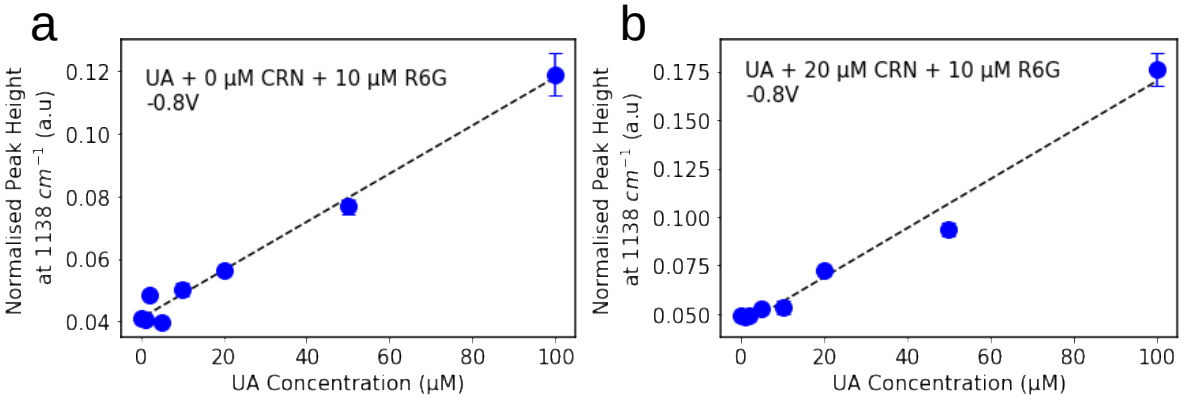

Fig. S12: (a) The R6G normalised peak height at 1138 cm^{-1} plotted against UA concentration for the spectra recorded at -0.8V. A linear relationship is fitted between UA concentration and the peak height for concentrations from 1 µM to 100 µM (R^2 = 0.988). (b) The R6G normalised peak height at 1138 cm^{-1} plotted against UA concentration for the spectra recorded at -0.8 V for a solution containing 20 µM CRN. A linear relationship is fitted between UA concentration and the peak height for concentrations from 1 µM to 100 µM (R^2 = 0.987). (RE: Ag/AgCl; WE: Ag NPs on FTO; CE: platinum plate; supporting electrolyte: 0.1 M NaF).

Table S1: Detection of uric acid by SERS or E-SERS reported in the literature.

Method	Material	Limit of detection (μM)	Linear range (μM)	Reference
SERS	Ag NPs	110	0 - 3500	[2]
SERS	Ag NPs	5	5 - 1000	[11]
SERS	Ag NPs	1.7	5 - 1000	[12]
SERS	Ag NPs/ZnO/Fe3O4	0.365	0.5 - 10	[13]
SERS	Au NP:CB7 nanoaggregates	0.2	0.2 - 10	[14]
E-SERS	Au nanopillars	0.001	0.01 - 100	[15]
E-SERS	Multi-layered Au NPs/Ag NPs	100	100 - 1000	[16]
E-SERS	Polycarbonate nanocone array decorated with Au NPs	0.087	0.1 - 100	[17]
E-SERS	Ag NPs	0.13	1 - 100	This study

Table S2: Detection of creatinine by SERS reported in the literature.

Method	Material	Limit of detection (μM)	Linear range (μM)	Reference
SERS	Ag NPs	88.40	88.40 - 2475	[18]
SERS	Jaffe complex on Ag film	25	25 – 150	[19]
SERS	Boron nitride/Au nanocomposite	10	10 - 200	[20]
SERS	Ag NPs	5	5 - 1000	[11]
SERS	Au NP-coated blu-ray DVD	1.77	1.77 – 8.84	[21]
SERS	Au NP:CB7 nanoaggregates	0.53	0.53 – 13.26	[22]
SERS	Nanoporous Au disk	0.1	0.1 - 100	[23]
SERS	Au dendritic nanostructure	0.97	17.7 - 2829	[24]
SERS	Polyelectrolyte multilayers over Au film	0.29	1 - 1000	[25]
E-SERS	Ag NPs	0.35	1 - 1000	This study

Table S3: Comparison of the prediction accuracies (R^2s) and root mean square errors of prediction (RMSEPs) of the different machine learning algorithms based on the full dataset (2348 spectra): partial least squares regression (PLSR), multilayer perceptron (MLP), and the two-step PLSR-MLP model.

Model	UA prediction accuracy (R^2)	CRN prediction accuracy (R^2)	UA RMSEP (μM)	CRN RMSEP (μM)
PLSR	0.81	0.62	12.82	170.68
MLP	0.83	0.66	12.39	163.72
PLSR-MLP	0.96	0.91	5.93	84.7

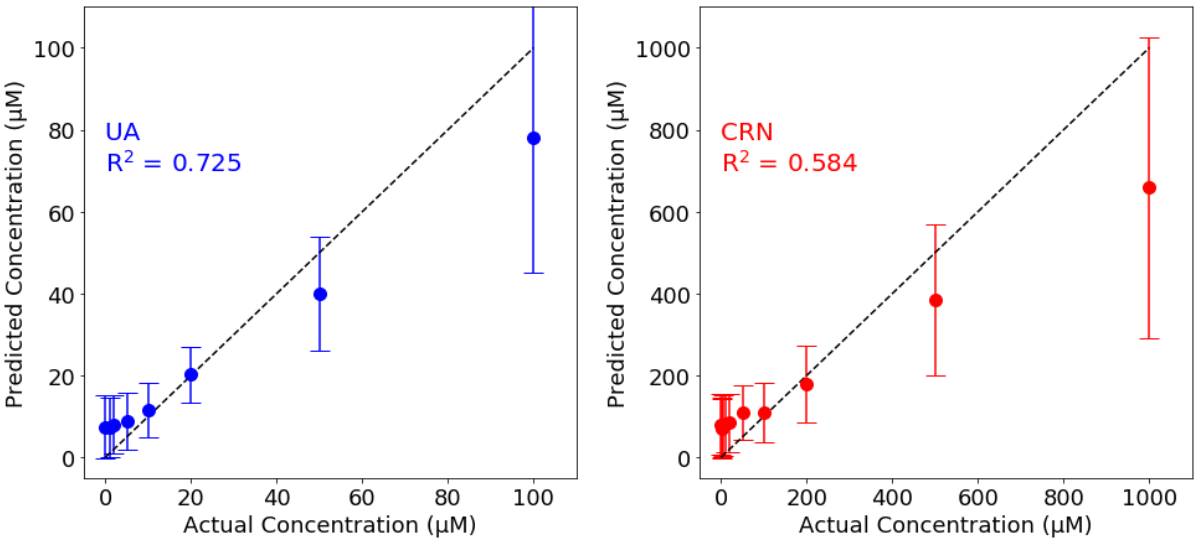

Fig. S13: A comparison of the actual concentrations and the predicted concentrations for the two-step PLSR-ANN model which was trained and tested using only the spectra recorded at 0V. The dotted y=x line represents perfect agreement between the actual and predicted concentrations.

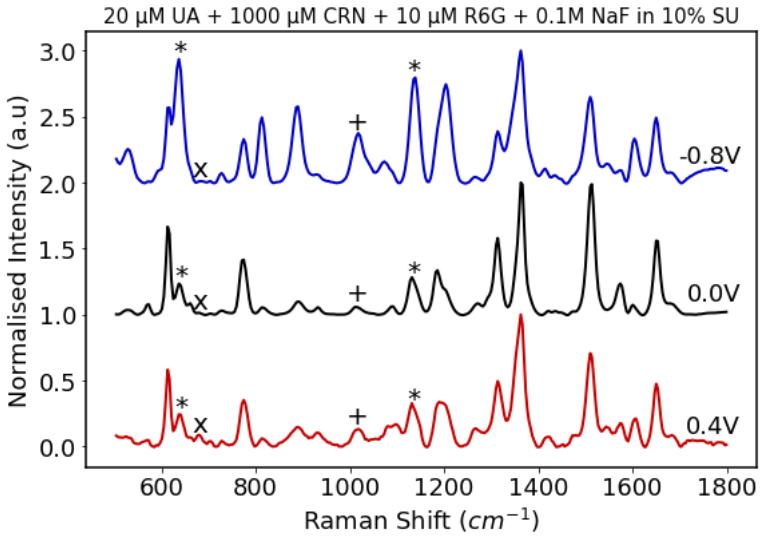

*Fig. S14: E-SERS spectra of a solution containing 20 μ UA, 1000 μM CRN, 10 μM R6G, and 0.1M NaF in a 10% synthetic urine solution. The characteristic UA, CRN and urea peaks are indicated with a *, x, and + respectively. (RE: Ag/AgCl; WE: Ag NPs on FTO; CE: Platinum plate; supporting electrolyte: 0.1 M NaF).*

References

1 P. C. Lee and D. Meisel, *J. Phys. Chem.*, 1982, **86**, 3391–3395.
2 J. E. L. Villa and R. J. Poppi, *Analyst*, 2016, **141**, 1966–1972.
3 B. R. Shmaefsky, *The American Biology Teacher*, 1990, **52**, 170–172.
4 F. Pedregosa, G. Varoquaux, A. Gramfort, V. Michel, B. Thirion, O. Grisel, M. Blondel, P. Prettenhofer, R. Weiss, V. Dubourg, J. Vanderplas, A. Passos, D. Cournapeau, M. Brucher, M. Perrot and É. Duchesnay, *Journal of Machine Learning Research*, 2011, **12**, 2825–2830.
5 P. H. C. Eilers, *Anal. Chem.*, 2003, **75**, 3631–3636.

6 S. Kasera, L. O. Herrmann, J. del Barrio, J. J. Baumberg and O. A. Scherman, *Sci Rep*, 2015, **4**, 6785.
7 R. L. Ott and M. T. Longnecker, *An Introduction to Statistical Methods and Data Analysis*, Cengage Learning, 2008.
8 I. Goodfellow, Y. Bengio and A. Courville, *Deep learning*, The MIT Press, Cambridge, Massachusetts, 2016.
9 J. Mockus, *J Glob Optim*, 1994, **4**, 347–365.
10 G. James, D. Witten, T. Hastie and R. Tibshirani, *An Introduction to Statistical Learning*, Springer New York, New York, NY, 2013, vol. 103.
11 Y. Lu, C. Wu, R. You, Y. Wu, H. Shen, L. Zhu and S. Feng, *Biomed. Opt. Express, BOE*, 2018, **9**, 4988–4997.
12 D. Lu, R. Cai, Y. Liao, R. You and Y. Lu, *Spectrochimica Acta Part A: Molecular and Biomolecular Spectroscopy*, 2023, **296**, 122631.
13 M. T. Alula, P. Lemmens, L. Bo, D. Wulferding, J. Yang and H. Spende, *Analytica Chimica Acta*, 2019, **1073**, 62–71.
14 W.-I. K. Chio, G. Davison, T. Jones, J. Liu, I. P. Parkin and T.-C. Lee, *JoVE*, 2020, 61682.
15 I. B. Ansah, W.-C. Lee, C. Mun, J.-J. Rha, H. S. Jung, M. Kang, S.-G. Park and D.-H. Kim, *Sensors and Actuators B: Chemical*, 2022, **353**, 131196.
16 L. Zhao, J. Blackburn and C. L. Brosseau, *Anal. Chem.*, 2015, **87**, 441–447.
17 C.-Y. Huang and H.-C. Hsiao, *Sensors (Basel)*, 2020, **20**, 7066.
18 Y. Wang, J. Chen, Y. Wu, Y. Chen, J. Pan, J. Lei, Y. Chen, L. Sun, S. Feng and R. Chen, in *Tenth International Conference on Photonics and Imaging in Biology and Medicine (PIBM 2011)*, SPIE, 2012, vol. 8329, pp. 142–148.
19 D. Gangopadhyay, P. Sharma, R. Nandi, M. Das, S. Ghosh and R. K. Singh, *RSC Adv.*, 2016, **6**, 112562–112567.
20 H. Zhang, G. Li, S. Li, L. Xu, Y. Tian, A. Jiao, X. Liu, F. Chen and M. Chen, *Applied Surface Science*, 2018, **457**, 684–694.
21 N. Chamuah, A. Saikia, A. M. Joseph and P. Nath, *Sensors and Actuators B: Chemical*, 2019, **285**, 108–115.
22 W.-I. K. Chio, S. Moorthy, J. Perumal, D. U. S., I. P. Parkin, M. Olivo and T.-C. Lee, *J. Mater. Chem. C*, 2020, **8**, 7051–7058.
23 M. Li, Y. Du, F. Zhao, J. Zeng, C. Mohan and W.-C. Shih, *Biomed Opt Express*, 2015, **6**, 849–858.
24 S. Azimi and A. Docoslis, *Sensors and Actuators B: Chemical*, 2023, **393**, 134250.
25 K. Karn-orachai and A. Ngamaroonchote, *Applied Surface Science*, 2021, **546**, 149092.